



ESVM : An Open-source Electrostatic Vlasov-Maxwell Code

Michaël J TOUATI^{1, 2, 3}

¹ Department of Electrical Engineering, University of California Los Angeles, Los Angeles, CA 90095, USA ² Group of Lasers and Plasmas, IPFN, IST, Universidade de Lisboa, Lisbon, Portugal ³ Centro de Láseres Pulsados de Salamanca (CLPU), Edificio M5, Parque Científico, C/ Adaja 8, 37185 Villamayor, Salamanca, Spain (current affiliation)

DOI: [10.21105/joss.03618](https://doi.org/10.21105/joss.03618)

Software

- [Review](#) 
- [Repository](#) 
- [Archive](#) 

Editor: [Daniel S. Katz](#) 

Reviewers:

- [@tclune](#)
- [@TomGoffrey](#)
- [@rouson](#)

Submitted: 11 August 2021

Published: 11 October 2021

License

Authors of papers retain copyright and release the work under a Creative Commons Attribution 4.0 International License ([CC BY 4.0](#)).

Summary

A plasma is a set of charged particles consisting of electrons and ionized atoms whose quantity is sufficiently large to behave collectively through the long-distance electromagnetic fields they produce. It is thought that more than 99.9% of visible matter in the Universe is in Plasma state. Consisting in an ionized gas composed of light electrons moving in between quasi-immobile positively charged and heavier ions on short time scales, any electrostatic field is rapidly screened over the Debye screening distance ([Debye & Hückel, 1923](#)) in a collisionless plasma. On such a short time scale or in very diluted plasmas where the number of electrons in these Debye spheres can be assumed to be infinite, the plasma electron population is correctly described by the Vlasov equation ([Vlasov, 1938](#)) that neglects all correlations between particles such as the binary Coulomb collisions between them. Besides its simplicity, the resulting Vlasov-Maxwell set of equations is extremely rich in Physics and has many applications ranging from Astrophysics and theoretical Plasma Physics to intense laser-matter interaction experiments. ESVM (ElectroStatic Vlasov-Maxwell) is a Vlasov-Maxwell standard-compliant Fortran code, parallelized with OpenMP and using Python 3 for post-processing, that allows for the study of these collisionless plasmas. Many finite volume numerical advection schemes ([Godunov, 1959](#)) are implemented in order to discretize the Vlasov equation, namely : - the donor-cell scheme i.e. the downwind / upwind scheme ([R. Courant et al., 1952](#)) depending on the advection direction in each phase-space cell, - the Lax-Wendroff scheme ([Lax & Wendroff, 1960](#)), - the Fromm scheme ([Fromm, 1968](#)), - the Beam-Warming scheme ([Beam & Warming, 1976](#)), - the Van Leer scheme ([Van Leer, 1977](#)), - the minmod scheme ([Roe, 1986](#)), - the superbee scheme ([Roe, 1986](#)) and - two Monotonic Upwind-centered Scheme for Conservation Laws (MUSCL) ([van Leer, 1979](#)) schemes MUSCL2 ([Crouseilles & Filbet, 2004](#)) and MUSCL1 ([Duclos et al., 2009](#)).

Contrary to the linear second order Lax-Wendroff, Fromm and Beam-Warming schemes, the non-linear second order minmod, superbee, Van Leer and MUSCL schemes make use of a Total Variation Diminishing (TVD) non-linear flux limiter with the price of becoming a first order scheme in some phase-space cells to limit the numerical oscillations. The donor-cell scheme is a first order method and has the pros of limiting such eventual oscillations but the cons of being numerically less consistent and more diffusive too. In ESVM, the discretized Vlasov equation is coupled with the self-consistent Maxwell-Gauss equation or equivalently with the Maxwell-Ampere equation with Maxwell-Gauss equation computed at the first time step, only. While the second order Maxwell-Gauss solver needs a computationally expensive inversion of a tridiagonal matrix for the computation of the Poisson equation, the Maxwell-Ampere equation solver makes use of a faster first order numerical scheme. Both absorbing and periodic boundary conditions for both the particles and the fields are implemented. Python scripts, using the Matplotlib and Numpy packages, are provided to automatically extract and

45 plot the stored simulation results. Compilation rules can be easily modified depending on the
46 user compiler preferences using the provided makefile. It is however recommended to compile
47 the code using the double-precision compiler option. Well known Plasma Physics academic
48 cases, tools for testing the compilation and tools for checking the simulation parameters that
49 are specified by the user in the input-deck are provided.

50 Statement of need

51 ESVM has been developed in order to adapt simulations to specific Plasma Physics problems
52 by choosing the more adequate finite volume numerical advection scheme in order to compute
53 the Vlasov equation phase-space advection derivatives and to choose between computing the
54 Maxwell-Gauss equation or the Maxwell-Ampere equation with Maxwell-Gauss equation com-
55 puted at the first time step, only. The code aims at being used by the open-source Highly
56 Parallel Computing (HPC) Plasma Physics community ranging from under or post-graduate
57 students to teachers and researchers who usually use Particle-In-Cell (PIC) codes (Dawson,
58 1962) to study collisionless plasmas. Indeed, the PIC method may prohibit the study of
59 Plasma Physical processes on large time scales and/or for very dense collisionless plasmas due
60 to the statistical and numerical fluctuations of the computed quantities imposed by the use of
61 a finite number of macroparticles. Also, plasma instabilities naturally develop in PIC codes,
62 seeded by the available fluctuations spatial spectrum k-vector for which the instability growth
63 rate is maximum and some small amplitude Plasma Physical processes may be hidden under
64 the fluctuations level. Compared to the many open source PIC code such as (Derouillat et
65 al., 2018) and semi-Lagrangian codes such as (de Buyl, 2014), there is no open source finite
66 volume Vlasov codes in the literature that are not based on an expansion method such as
67 (Tzoufras et al., 2011) (Touati et al., 2014) or (Joglekar & Levy, 2020). In addition, since
68 the Vlasov equation is a conservation equation of the number of particle in the phase-space,
69 using a finite volume method in order to compute the Vlasov equation presents the advantage
70 of allowing for the use of numerical schemes that are numerically flux conserving and/or that
71 ensure the distribution function positivity compared to other numerical methods. ESVM has
72 already been used during courses for under and post-graduate students about the “numerical
73 tools for laser-plasma interaction Physics” and it is currently used for theoretical Plasma
74 Physics investigations.

75 Equations computed by ESVM

76 Plasma ions are assumed to be immobile with a homogeneous density n_i and fully ionized
77 with an electrical charge Ze where Z is the plasma ion atomic number and e the elementary
78 charge. The plasma electron distribution function $f_e(x, v_x, t)$ is computed by ESVM according
79 to the plasma electron Vlasov equation

$$\frac{\partial f_e}{\partial t}(x, v_x, t) + \frac{\partial}{\partial x}(v_x f_e(x, v_x, t)) - \frac{\partial}{\partial v_x} \left(\frac{e}{m_e} E_x(x, t) f_e(x, v_x, t) \right) = 0 \quad (1)$$

80 that is self-consistently coupled with the Maxwell-Gauss equation

$$\frac{\partial E_x}{\partial x}(x, t) = 4\pi e (Zn_i - n_e(x, t)) \quad (2)$$

81 for the electrostatic field $E_x(x, t)$ or, equivalently, self-consistently coupled with the Maxwell-
82 Ampere equation

$$\frac{\partial E_x}{\partial t}(x, t) = -4\pi j_e(x, t) \quad (3)$$

with Maxwell-Gauss equation Equation 2 computed at the simulation start $t = 0$, only. Indeed, by integrating the plasma electron Vlasov equation Equation 1 over the whole plasma electron velocity space $v_x \in [v_{x,\min}, v_{x,\max}]$, one gets the hydrodynamic equation of plasma electron number conservation

$$\frac{\partial n_e}{\partial t}(x, t) + \frac{\partial}{\partial x} (n_e v_e(x, t)) = 0, \quad (4)$$

which, when injected in the time derivative of Maxwell-Gauss equation Equation 2, provides the Maxwell-Ampere equation Equation 3 if Maxwell-Gauss equation Equation 2 is verified at the simulation start $t=0$. Here,

$$n_e(x, t) = \int_{v_{x,\min}}^{v_{x,\max}} f_e(x, v_x, t) dv_x, \quad (5)$$

$$v_e(x, t) = \frac{1}{n_e(x, t)} \int_{v_{x,\min}}^{v_{x,\max}} f_e(x, v_x, t) v_x dv_x \quad (6)$$

and

$$j_e(x, t) = -en_e(x, t)v_e(x, t) \quad (7)$$

are the plasma electron density, mean velocity and electrical charge current, respectively. ESVM also computes the plasma electron thermal velocity $v_{T_e}(x, t)$ defined according to the plasma electron internal energy density

$$u_{T_e}(x, t) = \frac{n_e(x, t)}{2} m_e v_{T_e}(x, t)^2 = \frac{m_e}{2} \int_{v_{x,\min}}^{v_{x,\max}} f_e(x, v_x, t) (v_x - v_e(x, t))^2 dv_x. \quad (8)$$

For example, in 1D plasmas at local Maxwell-Boltzmann equilibrium, $v_{T_e}(x, t) = \sqrt{k_B T_e(x, t)/m_e}$ where k_B is the Boltzmann constant, $T_e(x, t)$ is the local electron temperature and m_e the electron mass. Maxwell-Gauss equation Equation 2 is computed by using the electrostatic potential definition

$$\frac{\partial \Phi}{\partial x}(x, t) = -E_x(x, t) \quad (9)$$

that gives the Poisson equation

$$\frac{\partial^2 \Phi}{\partial x^2}(x, t) = -4\pi e (Zn_i - n_e(x, t)) \quad (10)$$

for the electrostatic potential Φ when injected in the Maxwell-Gauss equation Equation 2. When the simulation is running, ESVM stores at every time steps and displays on the terminal at every dumped time steps t_d the total plasma electron internal and kinetic energy (assuming simulations with an area unit perpendicular to the x -axis of λ_{Debye}^2) and the total electrostatic energy in the simulation box $x \in [x_{\min}, x_{\max}]$

$$U_{T_e}(t_d) = \lambda_{\text{Debye}}^2 \int_{x_{\min}}^{x_{\max}} u_{T_e}(x, t_d) dx, \quad (11)$$

$$U_{K_e}(t_d) = \lambda_{\text{Debye}}^2 \int_{x_{\min}}^{x_{\max}} n_e(x, t) \frac{m_e v_e(x, t_d)^2}{2} dx \quad (12)$$

and

$$U_{E_x}(t_d) = \lambda_{\text{Debye}}^2 \int_{x_{\min}}^{x_{\max}} \frac{E_x(x, t_d)^2}{8\pi} dx, \quad (13)$$

respectively as well as the total energy

$$U_{\text{tot}}(t_d) = U_{T_e}(t_d) + U_{K_e}(t_d) + U_{E_x}(t_d) \quad (14)$$

in order to check the energy conservation in the simulation. The user can initialize : - an initial plasma electron population at Maxwell-Boltzmann equilibrium drifting at the velocity v_d

$$\begin{cases} f_e(x, v_x, t = 0) &= \frac{Zn_i}{\sqrt{2\pi v_{Te_0}^2}} \exp\left[-\frac{(v_x - v_d)^2}{2v_{Te_0}^2}\right] \\ E_x(x, t = 0) &= 0 \end{cases} \quad (15)$$

by no imposing any perturbation parameter or - a well known Plasma Physics process; cf. section **ESVM Plasma Physics academic case simulations**. - Finally, specific Plasma Physics simulations can easily be added in ESVM by implementing them in the Fortran 95 subroutine INIT_SIMU of the library.f90 source file.

ESVM units

The code units consist in the commonly used electrostatic units : the electron mass m_e for masses, the elementary charge e for electrical charges, the inverse of the Langmuir plasma electron angular frequency $\omega_p = \sqrt{4\pi Zn_i e^2 / m_e}$ for times, the Debye electron screening length $\lambda_{Debye} = v_{Te_0} / \omega_p$ and the constant electron density $n_0 = Zn_i$ for spatial densities. v_{Te_0} is therefore an important unit parameter of normalization since it fixes indirectly the space unit. It can be defined more generally as the initial plasma electron velocity distribution standard deviation if the plasma is not initialized at Maxwell-Boltzmann thermodynamic equilibrium; cf. Equation 8. Injecting these units in the equations computed by the code, one deduces the resulting normalized electrostatic field and electron distribution function that consequently reads $\underline{E}_x = eE_x / m_e \omega_p v_{Te_0}$ and $\underline{f}_e = f_e v_{Te_0} / n_0$, respectively.

ESVM numerical stability

The spatial grid cells should be chosen lower than the Debye length $\Delta x < \lambda_{Debye}$ for the simulation to be Physical. $v_{x,min}$ and $v_{x,max}$ should be chosen sufficiently large $|v_{x,min/max}| \gg v_{Te_0}$ in such a way that there is no plasma electrons outside the simulation velocity space during the whole simulation. The simulation velocity bin size should be chosen lower than the thermal electron velocity $\Delta v_x < v_{Te_0}$ and also sufficiently small to capture the desired Physics. The CFL stability condition (from the name of its finder R. Courant, K. Friedrichs and H. Lewy (R. Courant et al., 1928)) is implemented inside the code in such a way that the user just needs to specify in the input deck the scalar parameter $cfl < 1$ such that the normalized simulation time step reads

$$\Delta t_n = cfl \times F^n(\underline{\Delta x}, \underline{\Delta v_x}) < F^n(\underline{\Delta x}, \underline{\Delta v_x}) \quad (16)$$

at the time step $t_n = \sum_{m=1}^n \Delta t_m$ at time iteration n where $F^n(\underline{\Delta x}, \underline{\Delta v_x})$ depends on the chosen numerical scheme.

For example, if one notes

$$\underline{f}_e^{n,i} = \frac{1}{\underline{\Delta x}} \int_{\underline{x}_{i-1/2}}^{\underline{x}_{i+1/2}} \underline{f}_e(\underline{x}, t_n) d\underline{x} \quad (17)$$

the electron distribution function finite volume at the spatial location \underline{x}_i located in between $\underline{x}_{i-1/2} = \underline{x}_i - \underline{\Delta x}/2$ and $\underline{x}_{i+1/2} = \underline{x}_i + \underline{\Delta x}/2$ and one considers the Lax-Wendroff method to compute the advection

$$\frac{\partial \underline{f}_e}{\partial t} + \underline{v_x} \frac{\partial \underline{f}_e}{\partial \underline{x}} = 0 \quad (18)$$

of plasma electrons along the spatial \underline{x} -axis in the phase-space, the numerical scheme reads

$$\left[\frac{f_e^{n+1} - f_e^n}{\Delta t_n} \right]^i + v_x \left[\frac{F_x^{i+1/2} - F_x^{i-1/2}}{\Delta x} \right]^n = 0 \quad (19)$$

where the plasma electron fluxes across the volume sections located at $\underline{x}_{i\pm 1/2}$ are given by

$$F_x^{n,i+1/2} = \frac{f_e^{n,i+1} + f_e^{n,i}}{2} - \frac{v_x \Delta t_n}{\Delta x} \frac{f_e^{n,i+1} - f_e^{n,i}}{2} \quad (20)$$

and

$$F_x^{n,i-1/2} = \frac{f_e^{n,i} + f_e^{n,i-1}}{2} - \frac{v_x \Delta t_n}{\Delta x} \frac{f_e^{n,i} - f_e^{n,i-1}}{2}. \quad (21)$$

According to the Taylor expansion of $f_e^{n,i+i}$, $f_e^{n,i-i}$ and $f_e^{n+1,i}$ close to (\underline{x}_i, t_n) up to the third order in space and time, one can check the Lax-Wendroff numerical consistency error is indeed of second order :

$$\begin{aligned} \underline{\epsilon}^{n,i} &= \left[\frac{f_e^{n+1} - f_e^n}{\Delta t_n} \right]^i + v_x \left[\frac{F_x^{i+1/2} - F_x^{i-1/2}}{\Delta x} \right]^n - \left(\frac{\partial f_e}{\partial t} \Big|^{n,i} + v_x \frac{\partial f_e}{\partial x} \Big|^{n,i} \right) \\ &= \frac{\Delta t_n^2}{6} \frac{\partial^3 f_e}{\partial t^3} \Big|^{n,i} + v_x \frac{\Delta x^2}{6} \frac{\partial^3 f_e}{\partial x^3} \Big|^{n,i} + O(\Delta t_n^3 + \Delta x^3 + \Delta t_n \Delta x^2). \end{aligned} \quad (22)$$

By using the Von Neumann stability analysis, assuming periodic boundary conditions for simplicity and noting

$$\hat{f}_e^n(\underline{k}^p) = \frac{1}{N_x} \sum_{i=1}^{N_x} f_e^{i,n} \exp(-i \underline{k}^p \underline{x}_i) \Leftrightarrow f_e^{n,i} = \sum_{p=1}^{N_x} \hat{f}_e^n(\underline{k}^p) \exp(i \underline{k}^p \underline{x}_i) \quad (23)$$

with $\iota^2 = -1$, $N_x = 1 + (\underline{x}_{\max} - \underline{x}_{\min})/\Delta x$ the number of spatial grid points and $\underline{k}^p = 2\pi(p-1)/(\underline{x}_{\max} - \underline{x}_{\min})$ the discrete Fourier mode, one gets by injecting Equation 23 in Equation 19

$$\frac{\hat{f}_e^{n+1}(\underline{k}^p)}{\hat{f}_e^n(\underline{k}^p)} = 1 - \frac{v_x \Delta t_n}{\Delta x} \iota \sin(\underline{k}^p \Delta x) + \left(\frac{v_x \Delta t_n}{\Delta x} \right)^2 [\cos(\underline{k}^p \Delta x) - 1] \quad (24)$$

for each term p of the series. It implies the numerical scheme is stable,

$$\text{meaning } \left| \frac{\hat{f}_e^{n+1}(\underline{k}^p)}{\hat{f}_e^n(\underline{k}^p)} \right| < 1, \text{ if } \Delta t_n < \frac{\Delta x}{v_x}. \quad (25)$$

Performing the same reasoning when discretizing also the velocity space $\underline{v}_x^\ell = \underline{v}_{x,\min} + (\ell - 1)\Delta v_x$ with $N_{v_x} = 1 + (v_{x,\max} - v_{x,\min})/\Delta v_x$ velocity grid points and considering in addition the advection term of plasma electrons along the \underline{v}_x -axis in the velocity space for computing the Vlasov equation Equation 1 with each numerical scheme implemented in ESVM, one finds (sometimes empirically when it is too difficult analytically) that

$$F^n(\Delta x, \Delta v_x) = \frac{1/2}{\frac{\max_{\ell \in [1, N_{v_x}]} \{v_x^\ell\}}{\Delta x} + \frac{\max_{i \in [1, N_x]} \{\underline{E}_x^{n,i}\}}{\Delta v_x}}. \quad (26)$$

is a sufficient CFL stability condition for all numerical schemes implemented in ESVM to be stable.

ESVM Plasma Physics academic case simulations

Four well-known Plasma Physics academic cases are provided with ESVM : 1) the emission of an electrostatic wakefield by a Gaussian electron; cf. Figure 1 2) the linear Landau damping of an electron plasma wave; cf. Figure 2, 3) the non-linear Landau damping of an electron plasma wave; cf. Figure 3 and 4) the two-stream instability of two counter-propagating symmetric Gaussian electron beams; cf. Figure 4.

For each academic case, an example of input deck is provided together with one corresponding simulation result plot that the code typically generates. For 1), 2) and 3), the simulation is initialized assuming a non-drifting collisionless plasma at Maxwell-Boltzmann equilibrium

$$\begin{cases} f_e^{(0)}(x, v_x, t = 0) &= \frac{Zn_i}{\sqrt{2\pi v_{Te_0}^2}} \exp\left[-\frac{v_x^2}{2v_{Te_0}^2}\right] \\ E_x^{(0)}(x, t = 0) &= 0 \end{cases} \quad (27)$$

that is perturbed : - with a small perturbation

$$\delta f_e(x, v_x, t = 0) = A \frac{Zn_i}{2\pi\delta x\delta v} \exp\left[-\frac{(x - x_d)^2}{2\delta x^2}\right] \exp\left[-\frac{(v_x - v_d)^2}{2\delta v^2}\right], \quad (28)$$

consisting in a Gaussian electron located at $x_d = x_{\min} + (x_{\max} - x_{\min})/8$ with a standard deviation $\delta x = \lambda_{\text{Debye}}/4$ and drifting at a velocity v_d with a standard deviation $\delta v = v_{Te_0}/40$ at the simulation start $t = 0$ for 1), and - with a small perturbation consisting in a small amplitude electron plasma wave

$$\delta E_x(x, t < \delta t) = A \frac{m_e \omega_p v_{Te_0}}{e} \sin(\omega_0 t - kx) \quad (29)$$

propagating during a short time interval $\delta t = 6\pi/\omega_0$ after the simulation start $t = 0$ for 2) and 3).

Only the perturbation amplitudes $A < 1$ for 1), 2) and 3), the perturbation drift velocity $v_d > v_{Te_0}$ for 1) and the perturbation temporal and spatial angular frequencies ω_0 and k for 2) and 3) should be modified by the user when filling the input-deck in such a way that

$$\begin{cases} f_e(x, v_x, t) &= f_e^{(0)}(x, v_x, t) + \delta f_e(x, v_x, t) \\ E_x(x, t) &= E_x^{(0)}(x, t) + \delta E_x(x, t) \end{cases} \quad \text{with } |\delta f_e(x, v_x, t)| \ll f_e^{(0)}(x, v_x, t) \quad (30)$$

keeps being respected during the linear stage of the simulation. Except for non-linear Plasma Physics processes such as 3) for which the non-linear theory should be considered, the methodology that can be used to check any ESVM simulation results is always the same. Only analytical estimates used to check the ESVM simulation results of the provided academic case 4) are consequently detailed here in order to highlight it. The user can check the provided academic case simulation results 1), 2) and 3) by directly comparing the ESVM simulation results with the analytical estimates provided in (Decyk, 1987) (available at <https://picksc.idre.ucla.edu/wp-content/uploads/2015/04/DecykKyiv1987.pdf>) and in the reference textbooks (Landau & Lifshitz, 1981) and (Sagdeev & Galeev, 1969), respectively.

The provided Plasma Physics academic case 4) is initialized assuming two counter-propagating homogeneous Gaussian electron beams 'e, +' and 'e, -' of exactly opposite drift velocity $\pm v_d$ with same standard velocity deviation v_{Te_0}

$$f_e^{(0)}(x, v_x, t) = f_{e,+}^{(0)}(x, v_x, t) + f_{e,-}^{(0)}(x, v_x, t) \quad (31)$$

with

$$f_{e,\pm}^{(0)}(x, v_x, t) = \frac{Zn_i/2}{\sqrt{2\pi v_{Te_0}^2}} \exp\left[-\frac{(v_x \mp v_d)^2}{2v_{Te_0}^2}\right] \quad (32)$$

that is a solution of the Vlasov Equation Equation 1 and that doesn't produce any electrostatic fields

$$E_x^{(0)}(x, t) = 0 \quad (33)$$

according to Maxwell-Gauss Equation Equation 2. If one computes the Vlasov-Maxwell set of Equations {Equation 1, Equation 2} exactly, initializing it with the two-stream equilibrium distribution function Equation 31 without any perturbation, the counter-propagating electron beams would continue their propagation through the immobile plasma ions without any modification. In order to observe the two-stream instability,

$$f_e(x, v_x, t = 0) = f_e^{(0)}(x, v_x, t = 0) + \delta f_e(x, v_x, t = 0), \quad (34)$$

is initialized instead by adding a small perturbation

$$\delta f_e(x, v_x, t = 0) = \delta f_{e,+}(x, v_x, t = 0) + \delta f_{e,-}(x, v_x, t = 0) \quad (35)$$

on each beam of the form

$$\delta f_{e,\pm}(x, v_x, t = 0) = \pm A \sin(k_1 x) f_{e,\pm}^{(0)}(x, v_x, t = 0) \quad (36)$$

at the simulation start $t = 0$ with $A = 0.1$, $k_1 = 2\pi/L_x$ (parameter k in the input-deck) where $L_x = x_{\max} - x_{\min}$ can be modified by the user in the input-deck.

In order to get analytical estimates of growing plasma electron density and mean velocity and electrostatic fields in this ESVM simulation, one can linearize the Vlasov equation Equation 1 and the self-consistent Maxwell-Gauss equation Equation 2 computed by ESVM assuming the perturbation Equation 35 remains small compared to the equilibrium distribution Equation 31 during the simulation. They read

$$\frac{\partial \delta f_e}{\partial t} + \frac{\partial}{\partial x}(v_x \delta f_e) - \frac{e}{m_e} \frac{df_e^{(0)}}{dv_x} \delta E_x = 0 \quad (37)$$

and

$$\frac{\partial \delta E_x}{\partial x} = -4\pi e \int_{-\infty}^{\infty} \delta f_e dv_x, \quad (38)$$

up to the first order. Considering periodic boundary conditions, we may use a one-sided Fourier transformation in time (thus equivalent to a Laplace transform) and a Fourier series expansion in space for such a L_x -periodic initial condition problem. We will note

$$\hat{X}_p(t) = \frac{1}{L_x} \int_0^{L_x} X(x, t) \exp(+ik_p x) dx \Leftrightarrow X(x, t) = \sum_{p=-\infty}^{\infty} \hat{X}_p(t) \exp(-ik_p x) \quad (39)$$

with $\forall p \in \mathbb{Z}$, $k_p = 2\pi p/L_x$ and

$$\begin{aligned} \hat{\hat{X}}_p^{(+)}(\omega) &= \int_0^{\infty} dt \hat{X}_p(t) \exp(-i\omega t) \\ &= \int_0^{\infty} dt \int_0^{L_x} \frac{dx}{L_x} X(x, t) \exp[-i(\omega t - k_p x)] \\ \Leftrightarrow X(x, t) &= \int_{\iota R - \infty}^{\iota R + \infty} \frac{d\omega}{2\pi} \sum_{p=-\infty}^{\infty} \hat{\hat{X}}_p^{(+)}(\omega) \exp[+i(\omega t - k_p x)] \end{aligned} \quad (40)$$

where the integral in the complex ω -plane is taken along a straight line $\omega = \iota R$. By multiplying Equation 37 and Equation 38 by $\exp[-i(\omega t - k_p x)]/L_x$ and by integrating them from $x = -\infty$ to $x = \infty$ and from $t = 0$ to $t = \infty$, we obtain respectively

$$\hat{\hat{f}}_{e,p}^{(+)} = \frac{1}{\iota(\omega - k_p v_x)} \left[\hat{\hat{f}}_{e,p}(v_x, t = 0) + \frac{e}{m_e} \frac{df_e^{(0)}}{dv_x} \hat{\hat{E}}_{x,p}^{(+)} \right] \quad (41)$$

217 with

$$\widehat{\delta f}_{e,p}(v_x, t=0) = \alpha_p A \frac{Z n_i / 2}{\sqrt{2\pi v_{Te_0}^2}} \left\{ \exp \left[-\frac{(v_x - v_d)^2}{2v_{Te_0}^2} \right] - \exp \left[-\frac{(v_x + v_d)^2}{2v_{Te_0}^2} \right] \right\} \quad (42)$$

218 where

$$\alpha_p = \begin{cases} \mp 1/2\iota & \text{if } p = \pm 1 \\ 0 & \text{else} \end{cases} \quad (43)$$

219 and

$$\widehat{\delta E}_{x,p}^{(+)} = \frac{4\pi e}{\iota k_p} \int_{-\infty}^{\infty} \widehat{\delta f}_{e,p}^{(+)}(\omega, v_x) dv_x. \quad (44)$$

220 Injecting Equation 41 in Equation 44, we obtain the Fourier components of the electrostatic
221 field Laplace transform

$$\begin{aligned} \widehat{\delta E}_{x,p}^{(+)}(\omega) &= \frac{4\pi e}{k_p^2 \epsilon(\omega, k_p)} \int_{-\infty}^{\infty} \frac{\widehat{\delta f}_{e,p}(v_x, t=0)}{v_x - \omega/k_p} dv_x \\ &= \alpha_p \frac{A}{2\sqrt{2}} \frac{m_e v_{Te_0}}{e} \frac{Z \left(\frac{\omega/k_p - v_d}{v_{Te_0} \sqrt{2}} \right) - Z \left(\frac{\omega/k_p + v_d}{v_{Te_0} \sqrt{2}} \right)}{\epsilon(\omega, k_p) (k_p \lambda_{\text{Debye}})^2} \end{aligned} \quad (45)$$

222 where the plasma electrical permittivity reads

$$\begin{aligned} \epsilon(\omega, k) &= 1 - \frac{4\pi e^2}{m_e k^2} \int_{-\infty}^{\infty} \frac{1}{v_x - \omega/k} \frac{df_e^{(0)}}{dv_x} dv_x \\ &= 1 + \frac{1}{(k \lambda_{\text{Debye}})^2} \left\{ 1 + \frac{1}{2} \left[F \left(\frac{\omega/k - v_d}{v_{Te_0} \sqrt{2}} \right) + F \left(\frac{\omega/k + v_d}{v_{Te_0} \sqrt{2}} \right) \right] \right\} \end{aligned} \quad (46)$$

223 depending on the plasma dispersion function (Fried & Conte, 1961)

$$F(\zeta) = \zeta Z(\zeta) \text{ and } Z(\zeta) = \frac{1}{\sqrt{\pi}} \int_{-\infty}^{\infty} \frac{\exp(-z^2)}{z - \zeta} dz. \quad (47)$$

224 Since $v_d \gg v_{Te_0}$ in this ESVM simulation, we have the condition

$$\left| \frac{\omega}{k_p} \pm v_d \right| \gg v_{Te_0} \sqrt{2} \quad (48)$$

225 that is fulfilled for any given spatial frequency mode k_p and one thus may use the asymptotic
226 limit

$$F(\zeta) \underset{|\zeta| \gg 1}{=} \iota \zeta \sqrt{\pi} \exp(-\zeta^2) - 1 - \frac{1}{2\zeta^2} - \frac{3}{4\zeta^4} + O\left(\frac{1}{\zeta^6}\right) \quad (49)$$

227 that leads to the simpler dispersion relation

$$\epsilon(\omega, k) \underset{v_d \gg v_{Te_0}}{=} 1 - \frac{\omega_p^2}{2} \left[\frac{1}{(\omega - kv_d)^2} + \frac{1}{(\omega + kv_d)^2} \right] = 0 \quad (50)$$

228 retaining only the main term in the series expansion of the dispersion function Equation 47
229 up to the second order Equation 49. In this limit, the dispersion relation Equation 50 provides
230 four pure real solutions $\{\omega_1(k), \omega_2(k), \omega_3(k), \omega_4(k)\} \in \mathbb{R}^4$ for wavenumber k greater
231 or equal than the critical wavenumber ω_p/v_d . It means that the two counter-propagating
232 electron beams remain stable on space scales smaller than $2\pi v_d/\omega_p$. However, in the case
233 where $k_p < \omega_p/v_d$ considered here, one finds in addition to the two real poles

$$\omega_{1/2} \left(k < \frac{\omega_p}{v_d} \right) = \pm \omega_0(k) \quad (51)$$

234 where

$$\omega_0(k) = \omega_p \sqrt{\left(\frac{kv_d}{\omega_p}\right)^2 + \frac{1}{2} \left(1 + \sqrt{1 + 8\left(\frac{kv_d}{\omega_p}\right)^2}\right)} \underset{kv_d \ll \omega_p}{\sim} \omega_p, \quad (52)$$

235 two another pure imaginary conjugate poles

$$\omega_{3/4}(k < k_c) = \pm i\delta(k). \quad (53)$$

236 It means that the two counter-propagating electron beams streaming throught the immobile
237 plasma ions are unstable on space scales greater than $2\pi v_d/\omega_p$ and that this two-stream
238 instability grows exponentially at the rate

$$\delta(k) = \omega_p \sqrt{\frac{1}{2} \left(\sqrt{1 + 8\left(\frac{kv_d}{\omega_p}\right)^2} - 1 \right) - \left(\frac{kv_d}{\omega_p}\right)^2} \underset{kv_d \ll \omega_p}{\sim} |k| v_d. \quad (54)$$

239 The stable electron plasma waves angular frequency Equation 52 and the two stream instability
240 growth rate Equation 54 are plotted in Figure 5 as a function of the angular spatial frequency
241 mode k . Retaining the main terms in the series expansions of \mathcal{Z} up to the second order
242 in Equation 45 according to Equation 49, the Fourier components of the electrostatic field
243 Laplace transform simplify into

$$\widehat{\widehat{\mathbf{E}}}_{x,p}^{(+)}(\omega) \underset{v_d \gg v_{Te0}}{\sim} -\alpha_p A \frac{m_e v_d}{e} \frac{\omega_p^2}{\epsilon(\omega, k_p)(\omega - k_p v_d)(\omega + k_p v_d)}. \quad (55)$$

244 The poles of the Fourier components of the electrostatic fields Equation 55 are thus $\pm k_p v_d$
245 plus the ones of the plasma electrical permittivity Equation 50 given by Equations 51 and
246 Equation 53. We can now determine the time dependence of the spatial Fourier components
247 of the growing electrostatic field

$$\widehat{\widehat{\mathbf{E}}}_{x,p}(t) = \frac{1}{2\pi} \int_{\iota R - \infty}^{\iota R + \infty} \widehat{\widehat{\mathbf{E}}}_{x,p}^{(+)}(\omega) \exp(+i\omega t) d\omega \quad (56)$$

248 by using the residue theorem with the contour illustrated in Figure 6 in order to evaluate
249 the Cauchy principal value of this integral : since the function to integrate in Equation 56
250 is an analytic function of ω defined in the whole complex plane, we moved the contour of
251 integration usually taken slightly above the real axis into the lower half-plane sufficiently far
252 beneath the pole $-i\delta$ and passing round this pole and round the other poles lying above it in
253 such a way that it doesn't cross any of the poles of the function. We thus obtain

$$\begin{aligned} \widehat{\widehat{\mathbf{E}}}_{x,p}(t) &= A \frac{E_0}{2} \alpha_p \frac{\omega_p}{\omega_0(k_p)} \frac{\delta(k_p)^2 + (k_p v_d)^2}{\delta(k_p)^2 + \omega_0(k_p)^2} \sinh[\delta(k_p)t] \\ &+ A \frac{E_0}{2} \alpha_p \frac{\omega_p}{\omega_0(k_p)} \frac{\omega_0(k_p)^2 - (k_p v_d)^2}{\delta(k_p)^2 + \omega_0(k_p)^2} \sin[\omega_0(k_p)t] \end{aligned} \quad (57)$$

254 with

$$E_0 = \frac{m_e v_d \omega_p}{e} \quad (58)$$

255 that finally gives according to the Fourier series expansion Equation 39

$$\begin{aligned} \delta E_x(x, t) &= A \frac{E_0}{2} \alpha_p \frac{\omega_p}{\omega_0(k_1)} \frac{\delta(k_1)^2 + (k_1 v_d)^2}{\delta(k_1)^2 + \omega_0(k_1)^2} \sinh[\delta(k_1)t] \sin(k_1 x) \\ &+ A \frac{E_0}{2} \alpha_p \frac{\omega_p}{\omega_0(k_1)} \frac{\omega_0(k_1)^2 - (k_1 v_d)^2}{\delta(k_1)^2 + \omega_0(k_1)^2} \sin[\omega_0(k_1)t] \sin(k_1 x). \end{aligned} \quad (59)$$

256 Knowing the electrostatic field Equation 59, one may also deduce the perturbed distribution
257 function according to Equation 37. It reads

$$\begin{aligned}\delta f_e(x, v_x, t) &= \delta f_e(x, v_x, t=0) + \frac{e}{m_e} \frac{df_e^{(0)}}{dv_x}(v_x) \int_0^t \delta E_x[x + v_x(\tau - t), \tau] d\tau \\ &= f_{e,+}^{(0)}(v_x) \left[A \sin(k_1 x) + \frac{v_d - v_x}{v_{Te0}^2} \frac{e}{m_e} \int_0^t \delta E_x[x + v_x(\tau - t), \tau] d\tau \right] \\ &+ f_{e,-}^{(0)}(v_x) \left[-A \sin(k_1 x) - \frac{v_d + v_x}{v_{Te0}^2} \frac{e}{m_e} \int_0^t \delta E_x[x + v_x(\tau - t), \tau] d\tau \right].\end{aligned}\quad (60)$$

258 In the limit $k_p v_d \ll \omega_p$, they simplify into

$$\delta E_x(x, t) \underset{k_1 v_d \ll \omega_p}{\sim} A \frac{E_0}{2} \left[\sin(\omega_p t) + 4 \frac{k_1 v_d}{\omega_p} \sinh(k_1 v_d t) \right] \sin(k_1 x) \quad (61)$$

259 and

$$\begin{aligned}\underset{k_1 v_d \ll \omega_p}{\sim} & A \frac{v_d}{1 - \left(\frac{k_1 v_x}{\omega_p}\right)^2} \left\{ \frac{e}{m_e} \int_0^t \delta E_x[x + v_x(\tau - t), \tau] d\tau \right. \\ & \left. \frac{k_1 v_x}{\omega_p} \sin(\omega_p t) \cos(k_1 x) - [\cos(\omega_p t) - 1] \sin(k_1 x) \right\} \\ + & A \frac{v_d}{1 + \left(\frac{v_x}{v_d}\right)^2} \left\{ -\frac{v_x}{v_d} \sinh(k_1 v_d t) \cos(k_1 x) + [\cosh(k_1 v_d t) - 1] \sin(k_1 x) \right\}.\end{aligned}\quad (62)$$

260 We thus deduce in this limit

$$\begin{aligned}\delta n_e(x, t) &= \int_{-\infty}^{\infty} \delta f_e(x, v_x, t) dv_x \\ \underset{k_1 v_d \ll \omega_p}{\sim} & -\frac{A}{2} Z n_i \frac{k_1 v_d}{\omega_p} \left[\sin(\omega_p t) + 4 \frac{k_1 v_d}{\omega_p} \sinh(k_1 v_d t) \right] \cos(k_1 x)\end{aligned}\quad (63)$$

261 and

$$\begin{aligned}\delta v_e(x, t) &= \frac{1}{Z n_i} \int_{-\infty}^{\infty} v_x \delta f_e(x, v_x, t) dv_x \\ \underset{k_1 v_d \ll \omega_p}{\sim} & -\frac{A}{2} v_d \left[(\cos(\omega_p t) - 1) + \left(2 \frac{k_1 v_d}{\omega_p}\right)^2 (\cosh(k_1 v_d t) - 1) \right] \sin(k_1 x).\end{aligned}\quad (64)$$

262 The first term in the square brackets

$$\begin{cases} \delta n_{osc}(x, t) \underset{k_1 v_d \ll \omega_p}{\sim} -\frac{A}{2} Z n_i \frac{k_1 v_d}{\omega_p} \sin(\omega_p t) \cos(k_1 x) \\ \delta v_{osc}(x, t) \underset{k_1 v_d \ll \omega_p}{\sim} -\frac{A}{2} v_d (\cos(\omega_p t) - 1) \sin(k_1 x) \\ \delta E_{osc}(x, t) \underset{k_1 v_d \ll \omega_p}{\sim} \frac{A}{2} E_0 \sin(\omega_p t) \sin(k_1 x) \end{cases} \quad (65)$$

263 corresponds to space-charge oscillations of stationary electrostatic plasma waves excited by
264 the perturbation imposed on each electron beam. We are rather interested here in the second
265 term in the square brackets

$$\begin{cases} \delta n_{ins}(x, t) \underset{k_1 v_d \ll \omega_p}{\sim} -2A Z n_i \left(\frac{k_1 v_d}{\omega_p}\right)^2 \sinh(k_1 v_d t) \cos(k_1 x) \\ \delta v_{ins}(x, t) \underset{k_1 v_d \ll \omega_p}{\sim} -2A v_d \left(\frac{k_1 v_d}{\omega_p}\right)^2 (\cosh(k_1 v_d t) - 1) \sin(k_1 x) \\ \delta E_{ins}(x, t) \underset{k_1 v_d \ll \omega_p}{\sim} 2A E_0 \frac{k_1 v_d}{\omega_p} \sinh(k_1 v_d t) \sin(k_1 x) \end{cases} \quad (66)$$

corresponding to the exponentially growing electrostatic field due to the two-stream instability. These latter growing electron density, current density and electrostatic field perturbations Equation 66 can directly be compared with the ESVM simulation result. One can also check that if $A = 0$, all quantities cancel. That confirms that, contrary to PIC codes, the two counter-propagating electron beams would continue their propagation without any modification if we do not impose an initial perturbation on which the instability will grow in ESVM. Finally, one can estimate the trajectories (x_ℓ, v_ℓ) of one beam electron $\ell \in [1, N_e]$ with an arbitrary initial velocity $v_\ell(t=0) = v_0$ in the beam velocity distribution function and an initial position $x_\ell(t=0) = x_0$ close to $x = 0$ such that $k_1 x_0 \ll 1$. At the early stage of the instability, the growing electrostatic field component δE_{ins} is small compared to the stationary plasma wave δE_{osc} that oscillates in time at the Langmuir electron angular frequency ω_p . On such time scale $\omega_p t \sim 1$, the beam electrons are consequently mainly affected by this electrostatic field component

$$m_e \frac{dv_\ell}{dt} = -e\delta E_{\text{osc}}(x_\ell(t), t) \quad (67)$$

and their trajectory is thus given by

$$\frac{d^2 x_\ell}{dt^2} + \omega_p^2 \left(\frac{A k_1 v_d}{2 \omega_p} \right) \sin(\omega_p t) x_\ell(t) = 0, \quad (68)$$

assuming that $k_1 x_\ell(t) \ll 1$ remains valid at every time $t > 0$ if it is valid at $t = 0$ such that $\forall t, \sin[k_1 x_\ell(t)] \sim k_1 x_\ell(t)$. Recognizing the Mathieu Equation

$$\frac{d^2 x_\ell}{du^2} + [a - 2q \cos(2u)] x_\ell(u) = 0 \quad (69)$$

with $a = 0$ and $q = -Ak_1 v_d / \omega_p$ by doing the change of variable $u(t) = (-\pi/4) + (\omega_p t/2)$, we deduce

$$k_1 x_\ell(t) = k_1 x_c c_{e,0}[q, u(t)] + k_1 x_s s_{e,0}[q, u(t)] \quad (70)$$

and

$$v_\ell(t) = \frac{v_d}{2} \frac{\omega_p}{k_1 v_d} \{k_1 x_c c'_{e,0}[q, u(t)] + k_1 x_s s'_{e,0}[q, u(t)]\} \quad (71)$$

with

$$\begin{cases} k_1 x_c = + \frac{s'_{e,0}(q, -\pi/4) k_1 x_0 - s_{e,0}(q, -\pi/4) (2k_1 v_d / \omega_p) (v_0 / v_d)}{c_{e,0}(q, -\pi/4) s'_{e,0}(q, -\pi/4) - c'_{e,0}(q, -\pi/4) s_{e,0}(q, -\pi/4)} \\ k_1 x_s = - \frac{c'_{e,0}(q, -\pi/4) k_1 x_0 - c_{e,0}(q, -\pi/4) (2k_1 v_d / \omega_p) (v_0 / v_d)}{c_{e,0}(q, -\pi/4) s'_{e,0}(q, -\pi/4) - c'_{e,0}(q, -\pi/4) s_{e,0}(q, -\pi/4)} \end{cases}, \quad (72)$$

accounting for the initial conditions at $t = 0$. Here, $c_{e,a}(q, u)$ and $s_{e,a}(q, u)$ are respectively the even and odd solutions of Mathieu Equation Equation 69 and $c'_{e,a}(q, u)$ and $s'_{e,a}(q, u)$ their first order derivatives. According to Equation 70 and Equation 71, the beam electron trajectories in space are only slightly modified compared to their ballistic initial trajectory $x_0 + v_0 t$ with a velocity that oscillates around their initial value v_0 with amplitudes slightly increasing with time. As a consequence, each beam velocity dispersion slightly increases with its propagation distance until the growing component of the electrostatic field δE_{ins} becomes greater than δE_{osc} . When this occurs, the equation of motion

$$m_e \frac{dv_\ell}{dt} = -e\delta E_{\text{ins}}(x_\ell(t), t) \quad (73)$$

gives

$$\frac{1}{2} \left(\frac{v_\ell(t)}{v_d} \right)^2 - \frac{1}{2} \left(\frac{v_0}{v_d} \right)^2 = -2Ak_1 \int_0^t v_\ell(t) \sin[k_1 x_\ell(t)] \sinh(k_1 v_d t) dt \quad (74)$$

and

$$\frac{d^2 x_\ell}{dt^2} + 2k_1 v_d^2 \sinh(k_1 v_d t) \sin[k_1 x_\ell(t)] = 0. \quad (75)$$

The energy conservation Equation Equation 74 shows that, at the early stage of the instability, electrons having a positive velocity $v_\ell(t) > 0$ at a location $0 < x_\ell(t) < L_x/2$ as well as electrons having a negative velocity $v_\ell(t) < 0$ at a location $-L_x/2 < x_\ell(t) < 0$ are losing energy contrary to electrons having a negative velocity $v_\ell(t) < 0$ at a location $0 < x_\ell(t) < L_x/2$ or electrons having a positive velocity $v_\ell(t) > 0$ at a location $-L_x/2 < x_\ell(t) < 0$ that are earning energy. In order to determine such an electron trajectory according to its equation of motion Equation 75, one can assume in addition that $k_1 x_\ell(t) \ll 1$ remains valid at every time $t > 0$ if it is valid at $t = 0$ such that $\forall t, \sin[k_1 x_\ell(t)] \sim k_1 x_\ell(t)$ and consider time scales of the order of electrostatic plasma oscillations ω_p^{-1} so that we may consider $\sinh(k_1 v_d t) \sim \exp(k_1 v_d t)/2$. In this case, Equation 75 simplifies into

$$\frac{d^2 x_\ell}{dt^2} + (k_1 v_d)^2 \exp(k_1 v_d t) x_\ell(t) = 0. \quad (76)$$

Recognizing the differential Bessel Equation by doing the change of variable $v(t) = \exp(k_1 v_d t)$

$$\frac{d^2 x_\ell}{dv^2} + \frac{1}{v} \frac{dx_\ell}{dv} + \frac{1}{v} x_\ell(v) = 0, \quad (77)$$

the beam electron trajectories can be found readily. They read

$$k_1 x_\ell(t) = k_1 x_J J_0(2\sqrt{v(t)}) + k_1 x_Y Y_0(2\sqrt{v(t)}) \quad (78)$$

and

$$v_\ell(t) = -v_d \left[k_1 x_J J_1(2\sqrt{v(t)}) + k_1 x_Y Y_1(2\sqrt{v(t)}) \right] \sqrt{v(t)} \quad (79)$$

with

$$\begin{cases} k_1 x_J &= + \frac{Y_1(2) k_1 x_0 + Y_0(2) (v_0/v_d)}{J_0(2) Y_1(2) - J_1(2) Y_0(2)} \\ k_1 x_Y &= - \frac{J_1(2) k_1 x_0 + J_0(2) (v_0/v_d)}{J_0(2) Y_1(2) - J_1(2) Y_0(2)} \end{cases}, \quad (80)$$

accounting for the initial conditions at $t = 0$. Here, J_μ and Y_μ are the Bessel functions of the first and second kind of order μ respectively. Some of these beam electron orbits are plotted in Figure 7. We can see that the beam electrons are looping around the phase-space center $(x, v) = (0, 0)$ with a velocity amplitude increasing with their initial spatial distance from $x = 0$ in agreement with the ESVM simulation Figure 4.

ESVM Perspectives

It is planned in a near future to : 1) provide another Plasma Physics academic simulation about one BGK (from the name of its finder I. B. Bernstein, J. M. Greene and M. D. Kruskal) non linear electron plasma wave (Bernstein et al., 1957) 2) provide another Plasma Physics academic simulation about Plasma wave echo (Gould et al., 1967) 3) implement non-equally spaced phase-space cells 4) implement high order Weighted Essentially Non-Oscillatory (WENO) advection schemes (Liu et al., 1994) 5) compute the plasma ion Vlasov equation to allow for the ions to be mobile 6) implement MPI parallelization 7) implement vectorization 8) store the simulation results in hdf5 files instead of text files 9) extend the code to the relativistic regime : ESVM \Rightarrow RESVM for open source Relativistic ElectroStatic Vlasov-Maxwell code 10) implement a BGK (from the name of its finder P. L. Bhatnagar, E. P. Gross and M. Krook) collision operator (Bhatnagar et al., 1954) 11) extend the code to 1D-2V and 1D-3V phase-space electrostatic plasma simulations 12) implement the Landau (Landau, 1937) and Belaiev-Budker (Belaiev & Budker, 1956) relativistic collision operators using the Rosenbluth potentials (Rosenbluth et al., 1957) and their relativistic Braams-Karney extension (Braams & Karney, 1987) : (R)ESVM \Rightarrow (R)ESVFPMP for open source (Relativistic) ElectroStatic Vlasov-Fokker-Planck-Maxwell code 13) extend the code to electrostatic 2D-1V, 2D-2V and

333 2D-3V phase-space plasma simulations : (R)ESV(FP)M \Rightarrow (R)ESV(FP)M2 for open source
 334 (Relativistic) ElectroStatic Vlasov-(Fokker-Planck-)Maxwell in 2D 14) extend the code with
 335 the second order finite difference Yee scheme (Yee, 1966) to electromagnetic 2D-1V, 2D-2V
 336 and 2D-3V phase-space plasma simulations : (R)ESV(FP)M(2) \Rightarrow (R)EMV(FP)M(2) for open
 337 source (Relativistic) ElectroMagnetic Vlasov-(Fokker-Planck)-Maxwell (in 2D) 15) implement
 338 the Perfectly Matched Layer (PML) technique (Berenger, 1994) to absorb the electromagnetic
 339 fields at the spatial simulation box boundaries 16) deploy the code to GPU architectures.

340 Figures

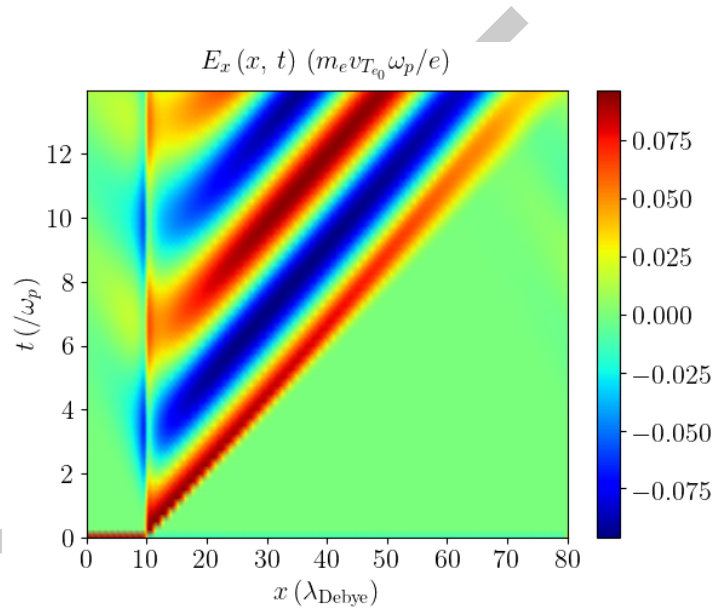


Figure 1: Electrostatic wakefield test case : Electrostatic wakefield $E_x(x, t)$ emitted by a Gaussian electron propagating in a collisionless plasma at Maxwell-Boltzmann equilibrium Equation 27 and initialized according to Equation 28 with $A = 0.1$ and $\underline{v_d} = 5$.

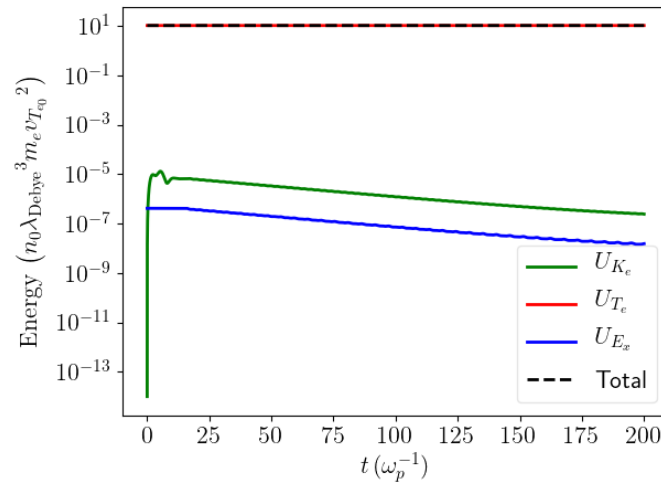


Figure 2: Linear Landau damping test case : Total electrostatic field energy and plasma electrons kinetic energy time evolution of the linearly Landau damped electron plasma wave propagating in the collisionless plasma at Maxwell-Boltzmann equilibrium Equation 27 and initialized according to Equation 29 with $A = 10^{-3}$, $\underline{k} = 0.29919930034$ and $\underline{\omega}_0 = 1.18$.

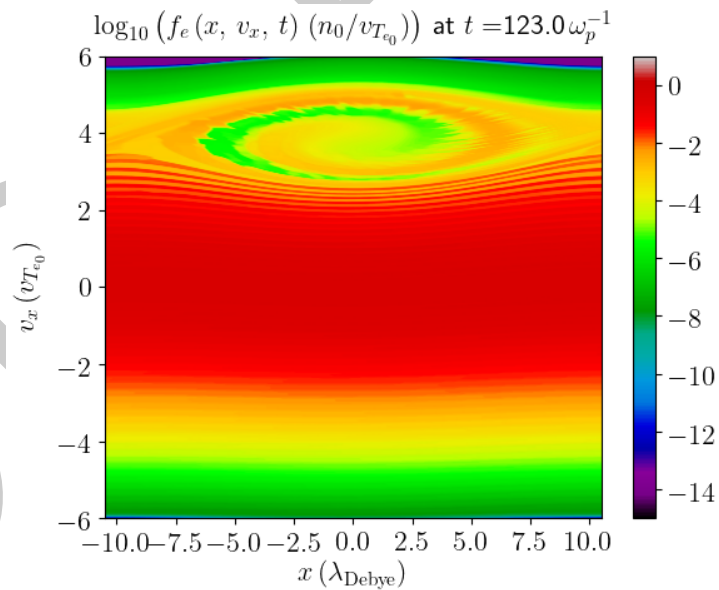


Figure 3: Non Linear Landau damping test case : Plasma electrons phase-space $\underline{f}_e(\underline{x}, \underline{v}_x, \underline{t} = 68)$ in the non-linear Landau damping of the electron plasma wave propagating in the collisionless plasma at Maxwell-Boltzmann equilibrium Equation 27 and initialized according to Equation 29 with $A = 10^{-1}$, $\underline{k} = 0.29919930034$ and $\underline{\omega}_0 = 1.18$.

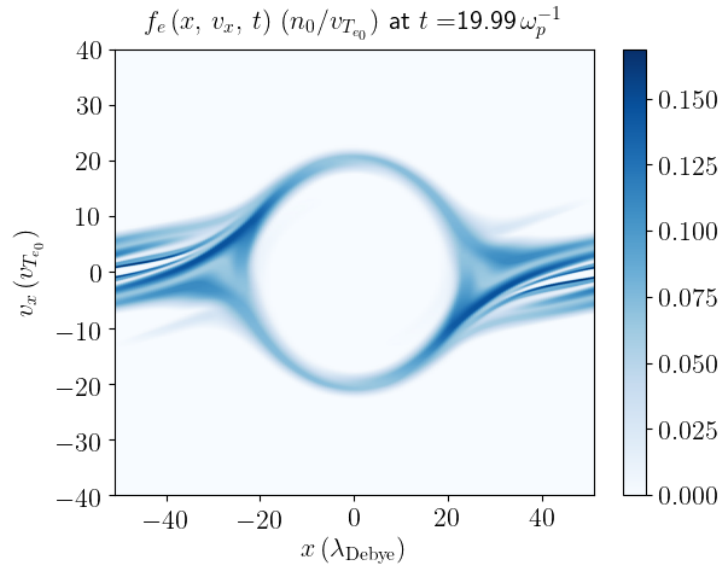


Figure 4: Two stream instability test case : Plasma electrons phase-space $f_e(\underline{x}, v_x, \underline{t} = 19.99)$ in the two-stream instability of two counter-propagating electron beams initialized according to Equation 34 with $A = 10^{-1}$, $\underline{k} = 0.06159985595$ ($x_{\min} = -x_{\max} = 51$) and $v_d = 10$.

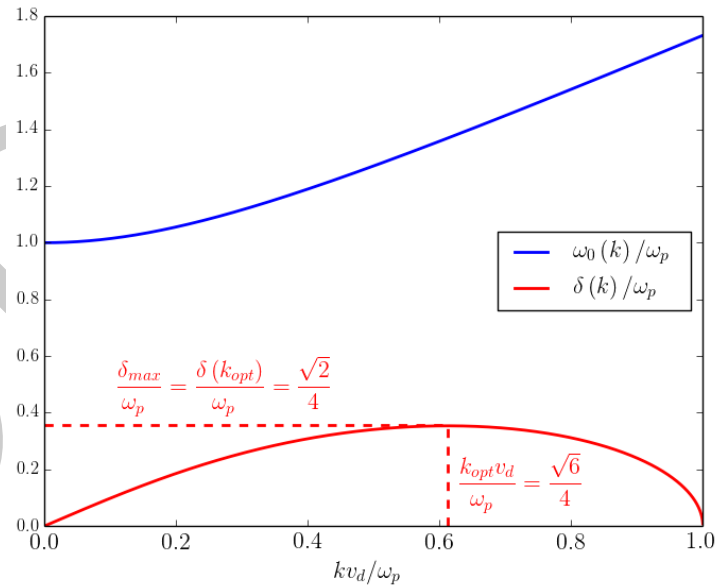


Figure 5: Two stream instability test case : Stationary electron plasma waves angular frequency Equation 52 seeded by the perturbation Equation 35 and the two-stream instability growth rate Equation 54 as a function of the spatial angular frequency mode k .

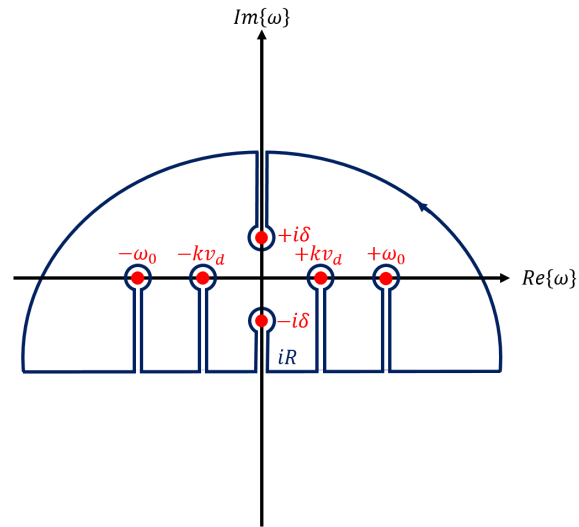


Figure 6: Two stream instability test case : Integration contour used to evaluate the the Cauchy principal value of the integral Equation 56.

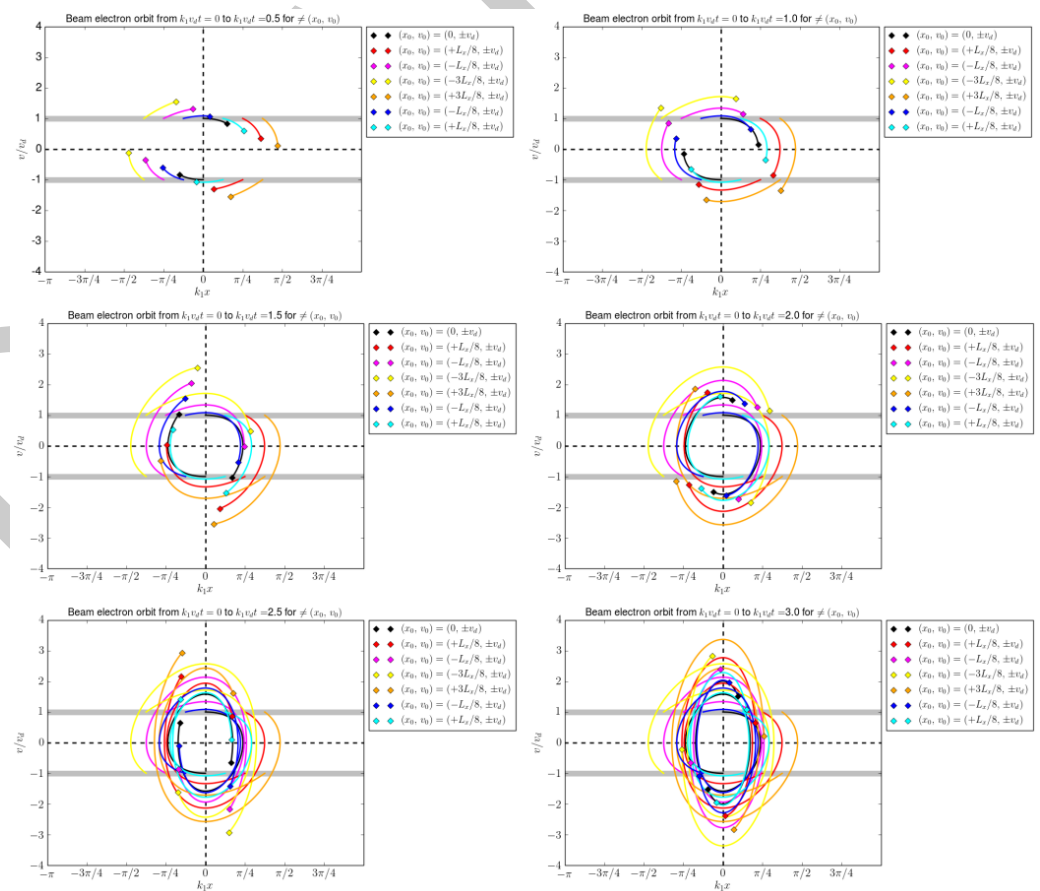


Figure 7: Two stream instability test case : Some beam electron orbits according to analytical estimates Equation 78 and Equation 79.

References

- Beam, R. M., & Warming, R. F. (1976). An implicit finite-difference algorithm for hyperbolic systems in conservation-law form. *Journal of Computational Physics*, 22(1), 87–110. [https://doi.org/https://doi.org/10.1016/0021-9991\(76\)90110-8](https://doi.org/https://doi.org/10.1016/0021-9991(76)90110-8)
- Belaiev, S. T., & Budker, G. I. (1956). *Dokl. Akad. Nauk SSSR*, 107.
- Berenger, J.-P. (1994). A perfectly matched layer for the absorption of electromagnetic waves. *Journal of Computational Physics*, 114(2), 185–200. <https://doi.org/https://doi.org/10.1006/jcph.1994.1159>
- Bernstein, I. B., Greene, J. M., & Kruskal, M. D. (1957). Exact nonlinear plasma oscillations. *Phys. Rev.*, 108, 546–550. <https://doi.org/https://doi.org/10.1103/PhysRev.108.546>
- Bhatnagar, P. L., Gross, E. P., & Krook, M. (1954). A model for collision processes in gases. I. Small amplitude processes in charged and neutral one-component systems. *Phys. Rev.*, 94, 511–525. <https://doi.org/https://doi.org/10.1103/PhysRev.94.511>
- Braams, B. J., & Karney, C. F. F. (1987). Differential form of the collision integral for a relativistic plasma. *Phys. Rev. Lett.*, 59, 1817–1820. <https://doi.org/https://doi.org/10.1103/PhysRevLett.59.1817>
- Courant, R., Friedrichs, K., & Lewy, H. (1928). Über die partiellen differenzengleichungen der mathematischen. *Physik. Math. Ann.*, 100, 32–74. <https://doi.org/https://doi.org/10.1007/BF01448839>
- Courant, R., Isaacson, E., & Rees, M. (1952). On the solution of nonlinear hyperbolic differential equations by finite differences. *Communications on Pure and Applied Mathematics*, 5(3), 243–255. <https://doi.org/https://doi.org/10.1002/cpa.3160050303>
- Crouseilles, N., & Filbet, F. (2004). Numerical approximation of collisional plasmas by high order methods. *Journal of Computational Physics*, 201(2), 546–572. <https://doi.org/https://doi.org/10.1016/j.jcp.2004.06.007>
- Dawson, J. (1962). One-dimensional plasma model. *The Physics of Fluids*, 5(4), 445–459. <https://doi.org/https://doi.org/10.1063/1.1706638>
- de Buyl, P. (2014). The vmf90 program for the numerical resolution of the vlasov equation for mean-field systems. *Computer Physics Communications*, 185(6), 1822–1827. <https://doi.org/https://doi.org/10.1016/j.cpc.2014.03.004>
- Debye, P., & Hückel, E. (1923). Zur theorie der elektrolyte. I. Gefrierpunktserniedrigung und verwandte erscheinungen. *Z. Phys.*, 24, 305–324.
- Decyk, V. K. (1987). Simulation of microscopic processes in plasma. *Proc. 1987 International Conference on Plasma Physics, Kiev, USSR, April 1987, Ed. A G Sitenko [World Scientific, Singapore, 1987] Vol. II, p. 1075.*
- Derouillat, J., Beck, A., Pérez, F., Vinci, T., Chiaramello, M., Grassi, A., Flé, M., Bouchard, G., Plotnikov, I., Aunai, N., Dargent, J., Riconda, C., & Grech, M. (2018). Smilei : A collaborative, open-source, multi-purpose particle-in-cell code for plasma simulation. *Computer Physics Communications*, 222, 351–373. <https://doi.org/https://doi.org/10.1016/j.cpc.2017.09.024>
- Duclous, R., Dubroca, B., Filbet, F., & Tikhonchuk, V. (2009). High order resolution of the maxwell-fokker-planck-landau model intended for ICF applications. *Journal of Computational Physics*, 228(14), 5072–5100. <https://doi.org/https://doi.org/10.1016/j.jcp.2009.04.005>
- Fried, B. D., & Conte, S. D. (1961). Elsevier.

- Fromm, J. E. (1968). A method for reducing dispersion in convective difference schemes. *Journal of Computational Physics*, 3(2), 176–189. [https://doi.org/10.1016/0021-9991\(68\)90015-6](https://doi.org/10.1016/0021-9991(68)90015-6)
- Godunov, S. K. (1959). Eine differenzenmethode für die näherungsberechnung unstetiger lösungen der hydrodynamischen gleichungen. *Mat. Sb., Nov. Ser.*, 47, 271–306.
- Gould, R. W., O'Neil, T. M., & Malmberg, J. H. (1967). Plasma wave echo. *Phys. Rev. Lett.*, 19, 219–222. <https://doi.org/10.1103/PhysRevLett.19.219>
- Joglekar, A. S., & Levy, M. C. (2020). VlaPy: A python package for eulerian vlasov-poisson-fokker-planck simulations. *Journal of Open Source Software*, 5(53), 2182. <https://doi.org/10.21105/joss.02182>
- Landau, L. D. (1937). *JETP*, 7, 203.
- Landau, L. D., & Lifshitz, E. M. (1981). *Physical kinetics* (Vol. 10). Pergamon Press.
- Lax, P., & Wendroff, B. (1960). Systems of conservation laws. *Communications on Pure and Applied Mathematics*, 13(2), 217–237. <https://doi.org/10.1002/cpa.3160130205>
- Liu, X.-D., Osher, S., & Chan, T. (1994). Weighted essentially non-oscillatory schemes. *Journal of Computational Physics*, 115(1), 200–212. <https://doi.org/10.1006/jcph.1994.1187>
- Roe, P. L. (1986). Characteristic-based schemes for the euler equations. *Annual Review of Fluid Mechanics*, 18(1), 337–365. <https://doi.org/10.1146/annurev.fl.18.010186.002005>
- Rosenbluth, M. N., MacDonald, W. M., & Judd, D. L. (1957). Fokker-planck equation for an inverse-square force. *Phys. Rev.*, 107, 1–6. <https://doi.org/10.1103/PhysRev.107.1>
- Sagdeev, R. Z., & Galeev, A. A. (1969). *Nonlinear Plasma Theory*. W. A. Benjamin, Inc., New York.
- Touati, M., Feugeas, J.-L., Nicolai, P., Santos, J. J., Gremillet, L., & Tikhonchuk, V. T. (2014). A reduced model for relativistic electron beam transport in solids and dense plasmas. *New Journal of Physics*, 16(7), 073014. <https://doi.org/10.1088/1367-2630/16/7/073014>
- Tzoufras, M., Bell, A. R., Norreys, P. A., & Tsung, F. S. (2011). A vlasov-fokker-planck code for high energy density physics. *Journal of Computational Physics*, 230(17), 6475–6494. <https://doi.org/10.1016/j.jcp.2011.04.034>
- van Leer, B. (1979). Towards the ultimate conservative difference scheme. V. A second-order sequel to godunov's method. *Journal of Computational Physics*, 32(1), 101–136. [https://doi.org/10.1016/0021-9991\(79\)90145-1](https://doi.org/10.1016/0021-9991(79)90145-1)
- Van Leer, B. (1977). Towards the ultimate conservative difference scheme III. Upstream-centered finite-difference schemes for ideal compressible flow. *Journal of Computational Physics*, 23(3), 263–275. [https://doi.org/10.1016/0021-9991\(77\)90094-8](https://doi.org/10.1016/0021-9991(77)90094-8)
- Vlasov, A. A. ;. (1938). *JETP*, 8(3), 291.
- Yee, K. (1966). *IEEE Transactions on Antennas and Propagation*, 14(3), 302–307. <https://doi.org/10.1109/TAP.1966.1138693>